International Journal for Modern Trends in Science and Technology, 9(06): 131-140, 2023

ISSN: 2455-3778 online
DOI: https://doi.org/10.46501/IJMTST0906020
Available online at: http://www.ijmtst.com/vol9issue06.html

Performance of Fuzzy based DVR for Standalone Hybrid PV-Wind Power System Using Battery

Mulumudi Rajesh[1] | Dr. Aithepalli Lakshmi Devi[2]

[1]Department of Electrical and Electronic Engineering, Sri Venkateswara University College of Engineering, Tirupati, Andhra Pradesh, India.
[2]Department of Electrical and Electronic Engineering, Sri Venkateswara University College of Engineering, Tirupati, Andhra Pradesh, India.

To Cite this Article
Mulumudi Rajesh and Dr. Aithepalli Lakshmi Devi. Performance of Fuzzy based DVR for Standalone Hybrid PV-Wind Power System Using Battery. International Journal for Modern Trends in Science and Technology 2023, 9(06), pp. 131-140. https://doi.org/10.46501/IJMTST0906020

Article Info
Received: 18 May 2023; Accepted: 15 June 2023; Published: 16 June 2023.

ABSTRACT

This research uses simulation to analyse the efficiency of a system that combines solar (PV), wind, and battery energy storage (BESS). Temperature, solar irradiance, and wind speed variations are factored into the study. The consequences of the hybrid system's random fluctuations due to weather changes are softened by the battery storage system. The DC hybrid system uses an inverter equipped with an LCL filter to connect to an AC non-linear load and sensitive loads. In this work, we present a new low-cost high-gain DC-DC boost converter. In compared to other previous presentations of high voltage gain DC-DC converters, the suggested converter in this study keeps the total number of components much lower while yet providing high DC voltage gain. The suggested converter achieves high-voltage gain with a minimum of components (one power switch, two inductors, two capacitors, and three diodes). In addition, when compared to alternative designs with the same power rating, the suggested design makes use of smaller passive component sizes. On the primary side, a boost type high-voltage gain DC-DC converter is controlled by fuzzy logic. In addition, the boost converter's operation is based on an incremental conductance method, which guarantees the highest possible power production from the PV array. To fix the voltage and current waveform distortion caused by AC non-linear and sensitive loads, a dynamic voltage restorer (DVR) is used. The proposed converter requires only a single power switch, two inductors, two capacitors, and three diodes to achieve its high voltage gain. In addition, the recommended layout uses less passive component sizes than other layouts with the same power rating. Since there is no need to connect to the grid, islanded hybrid RE systems are ideal for remote locations with low load factors. We create a hybrid system model and implement it in the simulation software MATLAB/Simulink. Different waveforms generated by the hybrid system are displayed and analysed based on the simulation findings.

KEYWORDS: photovoltaic system; wind energy system; BESS; hybrid RE system; interfacing inverter; non-linear and sensitive loads;

1. INTRODUCTION

The worldwide demand for energy increased by 2.9% last year, nearly twice the yearly growth rate of 1.5% experienced over the preceding decade [1]. The prediction by [2] for industrial sub-sectors (energy intensive manufacturing, non-energy intensive

manufacturing, and non-manufacturing) predicts a 50% growth in energy consumption in energy-intensive manufacturing businesses from 2018 to 2050. The concerns with greenhouse gas emissions, the scarcity of nonrenewable energy sources in nature, and the volatility of their prices make them unsuitable for meeting this energy need. Therefore, in order to meet future energy demands, it is imperative that RES, such as wind and solar PV electricity, be utilised in an efficient manner. In specifically, the 2050 energy transformation roadmap projects that wind and PV power sources will boost GDP by 2.5%, raise employment rate by 2%, increase energy efficiency by 30%, reduce CO2 petrol emissions by 70%, and meet energy demand at the lowest possible cost [3, 4]. Since RES are more widely available, environmentally friendly, cost-effective, and socially acceptable than fossil fuel resources [5], they should meet two-thirds of the world's energy needs [3, 4, 6]. Many nations are looking to reduce their reliance on nonrenewable energy sources and their associated environmental implications by meeting much of their energy needs through renewable means [7]. In light of the findings of studies [3, 4], [8] - [11], this will constitute the actualization of the 2050 road map of the International Renewable Energy Agency. There should be appropriate solutions to alleviate the power fluctuation problems faced by end users due to the intermittent nature of RESs [12], despite the fact that their use is the bright future in the transition away from non-renewable energy sources. Its dependence on atmospheric factors including wind speed and solar irradiation accounts for most of its unpredictability [6, 9], [12], [13]. Power companies and customers should take into account the fact that most modern industrial load types, such as those used in semiconductor manufacturing and chemical processing, are extremely sensitive to power fluctuations [14], [15]. Dynamic voltage restorers (DVRs) are the most cost-effective and all-encompassing type of CPDs that may be used for this purpose, and they will be coupled in series or shunt at the sensitive load side [14], [16]-[19]. DVRs are used to prevent essential consumer loads from tripping and incurring losses due to main power quality (PQ) issues such as voltage sag, swell, interruptions, harmonics, and flickers [16, 20], [21]. A remote bus problem, switching heavy loads, starting large motors, or energising a transformer can all lead to voltage disturbances, the most common of which is sag. There's also a sudden change in phase angle because of this [19]. In the case of a PV-wind power system, sag may also be the result of sources that are intermittent. To reduce the overall converter loss compared to a single-stage system, single-switch converters are commonly employed in two-stage SETSs. DC-DC converter losses are insignificant in light of the system's robustness and maximum power point tracking [22]. Moreover, a boost converter fed from a smaller array is a suitable solution to avoid the sequential addition of a large number of panels due to the hot spot issue. Therefore, in this paper, a two-stage SETS is created to keep the system stable. It has been stated that the most common MPPT methods (hill climbing, P&O, IC) are able to maximise power extraction while requiring minimal operator effort. However, under conditions of partial shade of PV panels, they are unable to identify the global peak [23]. The speed and precision of the control also depend critically on the search's initial condition and the size of its steps. There are reports of more sophisticated MPPT algorithms that manage to get over the partial shading problem, but these methods add complexity to the control system [24]. Reviewing the literature, one discovers that modern AI, particle swarm optimisation, fuzzy logic, etc. [25] are effective but difficult to implement. At the MPP, P&O oscillates, leading to system-wide oscillation. A two-stage system employing the IC-MPPT algorithm provides a compromise between the two, though [26]-[27].

When high-voltage gain is needed but space is limited, a DC-DC boost converter is proposed as a feasible option in this paper. The proposed converter has a much smaller component count compared to some recently suggested high-voltage gain DC-DC converter designs [28], consisting of only one power switch (a power MOSFET), three diodes, two inductors, and two capacitors. Using a cascade structure, the authors of report a significant DC voltage gain. Following a quadratic boost converter, which generates a high voltage gain, comes a Cuk converter. Alterations to the DC bus bar in fuel-cell vehicles are one potential implementation of this strategy for achieving the sought-after effects. However, much more hardware is required for high-voltage gain. The converter uses only a single power switch, but the inclusion of three inductors, four diodes, and four capacitors makes the system

bulkier and less efficient. The non-linear AC loads are connected to the DC-coupled hybrid RE system via an inverter and LCL filter [29]. The algorithm for controlling the system is based on synchronous phase locked loop (PLL) technology and vector decoupling. The LCL filter provides a low-impedance channel for the inverter's high-frequency switching harmonics. With the proliferation of power electronics (PE) based loads like UPSs, laptops, LEDs, etc. at the load end, non-linearity in the system increases dramatically and injects harmonics [30]. on ensure the proposed system can handle a delicate load, we apply a non-linear load on it. A shunt connection is made for the non-linear load after the LCL filter, whereas the sensitive-load is connected at the load end. When a non-linear load is connected to a renewable energy system's power electronic (PE) interface, power quality (PQ) issues might develop. It is proposed to install a DVR based on the instantaneous symmetrical component theory (ISCT) at the connection point in order to eliminate PQ problems with the load voltage. Pulse width modulation is used by a voltage controller to generate the switching pulses that power the interface inverter. The LCL filter is followed by a connecting point at the AC bus. The non-linear load is wired to the DVR through a coupling transformer at this stage. The hybrid RE system for an island is represented as a Simulink model in Figure 2.

2. HYBRID RENEWABLE ENERGY STORAGE SYSTEM

The performance of each separate RE system is examined to accurately assess the operation of the hybrid RE system. Panel, Wind, and Battery Energy Storage (BESS) systems make up the hybrid RE system's DC design. Both the PV and WE systems are vulnerable to the ever-changing climate. The DC bus is directly connected to the PV array's high gain dc-dc boost converter, while the AC-DC converter links the DC bus to the WE generator and the battery. The DC bus voltage is adjusted such that it corresponds with the AC load voltage at the load end. At the point of connection, the rated voltage and frequency are both controlled by the interface inverter, which is built for DC-AC conversion. A voltage source converter links the DC bus to the storage battery that serves to maintain the bus voltage.

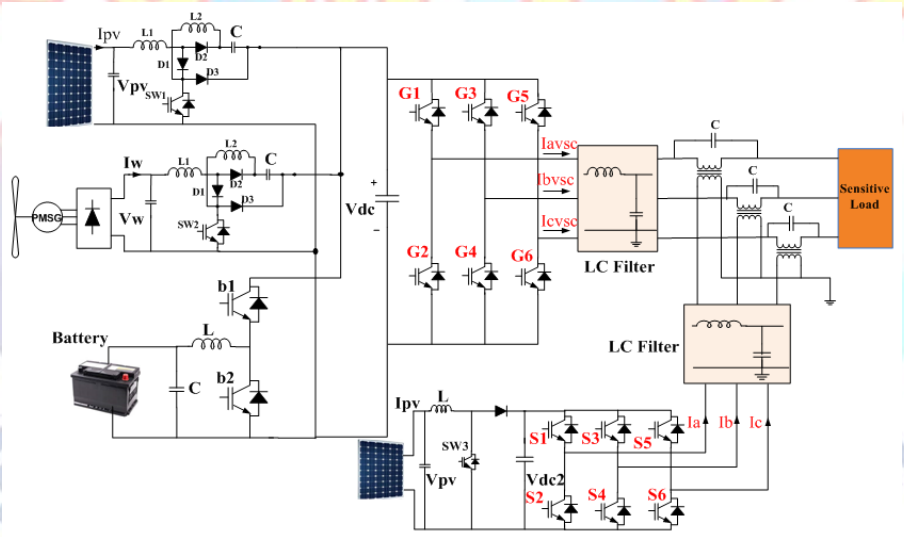

Fig. 1. Simulink model of proposed hybrid RE system

A. Photovoltaic System

Multiple solar panels connected in series and parallel make up a PV array. Solar irradiation, the orientation of the PV modules, and the temperature of the cells all influence the system's output power. PV arrays, a DC-DC converter, and a control circuit make up the PV system's three main components.

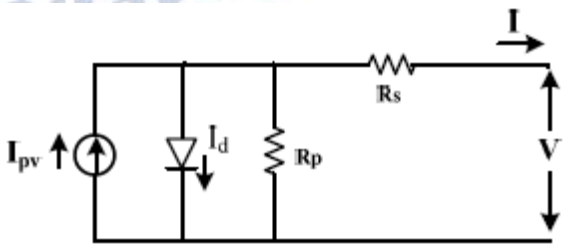

Fig. 2. Equivalent circuit diagram of a PV cell

The following equations describe a PV array in detail. An ideal expression for a PV cell's current–voltage (I–V) curve is

$$I = I_{Pv,cell} - I_{0,cell}\left[\exp\left(\frac{qv}{akT}\right) - 1\right] \quad (1)$$

Where

$I_{Pv,cell}$ = Solar photovoltaic cell current,

I_d = diode current

$I_{0,cell}$ = reverse saturation current of the diode

q = electron charge

K = Boltzmann constant

T = temperature in Kelvin

a = diode ideality factor.

To model a real-world PV array, however, you'll need to know how many modules will need to be wired in series and parallel to produce the needed amount of operating power. An actual PV array's I-V relationship can be calculated using

$$I = I_{PV} - I_0\left[\exp\left(\frac{V+R_sI}{V_t a}\right) - 1\right] - \frac{V+R_sI}{R_P} \quad (2)$$

where

Rs, Rp = equivalent series and parallel resistances of the PV array,

Ipv, I_0= PV and saturation currents of the array

Nss = modules in series

Npp = modules in parallel

And Ipv and I_0 may be defined as $I_{PV} = I_{PV}$, cell N_{pp} ; $I_0 = I_{PV}$, cell N_{pp}

With N_{ss} and N_{pp} modules connected in series and parallel, the Rs and Rp may be expressed as $\left(\frac{N_{ss}}{N_{pp}}\right)R_s$ and $\left(\frac{N_{ss}}{N_{pp}}\right)R_p$ respectively.

PV cell current is proportional to the square of the solar irradiation and the temperature, expressed as

$$I_{PV} = \left(I_{PV,n} + K_I\Delta T\right)\frac{G}{G_n} \quad (3)$$

where

pv,n I = light generated current at the nominal condition

G, Gn = actual and standard irradiances received by PV cell

KI = current coefficient

In ΔT = T − Tn , T and Tn are the actual and standard temperatures respectively.

The diode saturation current depends on temperature and is expressed as

$$I_0 = \frac{I_{sc,n}+K_I\Delta T}{\exp\left(\frac{V_{0c,n}+K_V\Delta T}{aV_t}\right)-1} \quad (4)$$

where

K v = voltage coefficient

I o = diode saturation current

Isc,n = rated short circuit current

Voc,n = rated open circuit voltage

t V = thermal equivalent voltage

Combining (3) and (4), the output current is given By

$$I = I_{PV}N_{PP} - I_0N_{PP}\left[\exp\left[\frac{V+R_s\left(\frac{N_{ss}}{N_{PP}}\right)}{V_t a N_{ss}}\right] - 1\right]\frac{V+R_s\left(\frac{N_{SS}}{N_{PP}}\right)}{R_p\left(\frac{N_{SS}}{N_{PP}}\right)}\ \mathrm{I} \quad (5)$$

where

I = output current

V = output voltage

A DC-DC boost converter with maximum power point tracking is used to get the most energy out of the PV array while also maintaining a constant DC voltage. Maximum power point tracking is being accomplished using aperturb and observation (P&O) technique. It is possible to calculate the duty cycle of the boost converter using

$$\frac{V_0}{V_i} = \frac{T_s}{t_{0ff}} = \frac{1}{1-D} \quad (6)$$

B. Wind Energy System

The WE system consists of a wind turbine, a wind generator, and an ACDC converter. This power supply uses a CAG with a damaged rotor. Estimating wind turbine power production is as

$$P_m = C_p(\lambda,\beta)\frac{1}{8}\rho\Pi\, d^2V^3 \quad (7)$$

where

Pm = mechanical power output of wind turbine (W)

ϱ = air density (kg/m3)

A = swept area of rotor (m2)

v = wind speed (m/s2)

cp = power coefficient

λ = tip speed ratio

β = rotor pitch angle

The tip speed ratio is given by

$$\lambda = \frac{\omega R}{v} \quad (8)$$

where

ω = angular velocity turbine

R = radius of the rotor

The rotor torque output, Tw is given by

$$T_w = \frac{C_p(\lambda,B)\frac{1}{8}\rho\Pi\, d^2v^3}{\omega} \quad (9)$$

The power coefficient, C_P can be defined as

$$c_P(\lambda,\beta) = C_1\left(\frac{C_2}{\lambda_i} - C_3\beta - C_4\right)e^{-5/\lambda_i} + C_6\lambda \quad (10)$$

where

c1 = 0.5176,c2 =116,c3 = 0.4,c4 = 5,c5 = 21,c6 = 0.0068

$$\frac{1}{\lambda_i} = \frac{1}{\lambda+0.08\beta} - \frac{0.035}{1+\beta^3} \qquad (11)$$

Fig. 3 is a plot of the power output from a wind turbine. For any given wind speed, there is a corresponding rotor speed that generates maximum power. The wind generator's alternating current (AC) voltage output is rectified using a three-phase diode rectifier. In addition, the DC output voltage is regulated using a DC-DC converter. The WE system's results under varying wind conditions are depicted in Fig. 10. The initial setting for the generator speed is 160 rad/s. At 415 V rms, the generator voltage causes a decrease in speed after 0.3 s. Because of its role as a generator, the asynchronous machine has a negative electromagnetic torque.

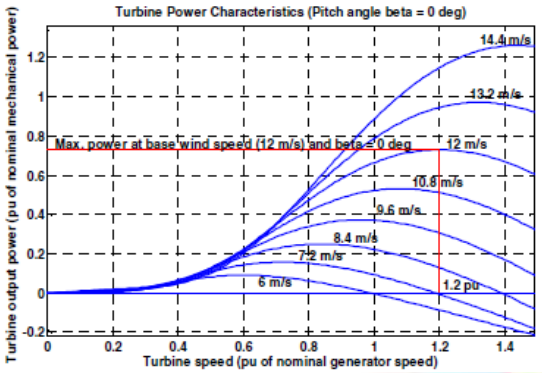

Fig. 3. Wind Turbine power curve

3. CONVERTERS MODELLING

1. Designing for DC-DC High Gain Boost Converter

The behaviour and performance of the device are profoundly affected by the design of the energy storage component, regardless of the DC-DC converter's architecture. By minimising the ripple current of inductors and the ripple voltage of capacitors, the DC voltage levels at the output can be made smoother and easier to manage. As a matter of thumb, an inductor's maximum current should be no more than 10% of the maximum current that might travel through the inductor. Maximum ripple voltage across a capacitor shouldn't exceed 10% of that which can build up across it. These parameters help in determining the appropriate size of inductors and capacitors for a reliable design that maintains a constant current and a uniform voltage throughout the load. The boost converter's computed inductor and capacitor values are shown in fig. 4.

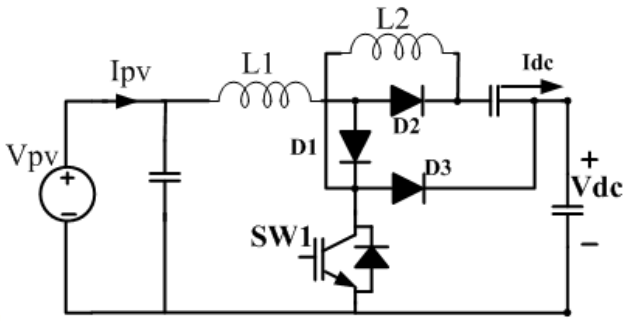

Fig. 4 a Novel High-Gain DC-DC Boost Converter

1.1 Design of Inductor L1

An inductor's voltage drop can be determined using

$$V_{in} = L\frac{dI_{L1}}{dt} \qquad (12)$$

This leads to the following expression for the current in inductor L1:

$$\Delta I_{L1} = \frac{V_{in}\cdot D\cdot T}{L1} \qquad (13)$$

A similar expression for the current in inductor L2 is

$$\Delta I_{L2} = \frac{V_{C1}\cdot D\cdot T}{L2} \qquad (14)$$

Calculating the potential difference across capacitor C1:

$$V_{C1}\cdot D\cdot\frac{1}{L2\cdot f_s} = v_{in}\left(\frac{D}{1-D}\right)\cdot\frac{1}{L2\cdot f_s} \qquad (15)$$

From (3),

$$\Delta I_{L2} = V_{C1}\cdot D\cdot\frac{1}{L2\cdot f_s} \qquad (16)$$

Comparing (4) and (5) gives

$$\Delta I_{L2} = V_{in}\cdot\frac{D}{1-D}\cdot\frac{1}{L2\cdot f_s} \qquad (17)$$

From (2), and in terms of Vout and fs

$$L1 = \frac{V_{out}\,(1-D)^2\cdot D}{\Delta I_{L1} f_s} \qquad (18)$$

(18) gives the minimum workable value for the L1 inductor. The DC voltage produced by the converter is denoted by Vout, the duty-cycle is indicated by D, and the switching frequency of the power switch is fs. I_L1 represents the oscillation of the current via the L1 inductor.

1.2. Design of Inductor L2

From (17),

$$L2 = \frac{V_{in}\cdot D}{\Delta I_{L_2}\cdot(1+D)\cdot f_s} \qquad (19)$$

Where I_L2 is the ripple current in the L2, and Vin and Vout are the input and output voltages, respectively.

1.3. Design of Capacitor C1

The current via the series-connected L2 and C1 in Mode 0 is calculated as

$$I_{C1} = C1\cdot\frac{\Delta V_{C1}}{\Delta t} \qquad (20)$$

In Mode 0, this equation looks like this:

$$C1 = \frac{I_0\cdot D\cdot T}{\Delta V_{in}} \qquad (21)$$

using the relation $V_{C1} = V_{in} \cdot \left(\frac{1}{1-D}\right)$ (22)

$$\frac{\Delta V_{C1}}{\Delta V_{in}} = \frac{1}{1-D}$$

Hence (10) becomes

$$C1 = \frac{I_0 \cdot D}{\Delta V_{C1} \cdot (1-D) \cdot f_s} \quad (23)$$

The minimal value of C1 that can be used with ΔV_c1 waves in the voltage across C1 is given by the relationship (23).

1.4. Design of Capacitor Co

The value of the current flowing through capacitor C2 is:

$$I_{Co} = Co \cdot \frac{dV_{out}}{dt} \quad (24)$$

In Mode 0

$$Co = I_{Co} \cdot \frac{D}{\Delta V_{out} \cdot f_s} \quad (25)$$

The equation (14) gives the minimum value of the output capacitor when the output voltage has ripples of V_Out t. If the switching frequency, output voltage ripple, and the output capacitor current are all held constant, the maximum value of the output capacitor is determined by the converter's duty-cycle. The output capacitor requires full duty-cycle operation of the converter.

2. Interfacing Inverter Control

Vector decoupling [31, 32] is used to regulate the inverter. An external voltage loop and an internal current loop work together to create the pulses in this technique. Block diagram of the suggested control mechanism is shown in Fig. 5. The PLL is utilised to get the angle, while Park's transformation is used to get the d-q components of the PCC voltages (Vd and Vq) and PCC currents (Id and Iq). The inner current loop of the d-q frame is split into two voltage loops, one of which regulates the DC-link bus voltage, Vdc, and the other of which regulates the PCC bus voltage and/or the AC bus voltage. The voltage and current control loops both use PI controllers to implement regulation. The decoupling term "L" in the present control loop allows for independent regulation of active and reactive power at PCC. Voltage, frequency, active, and reactive power regulation at the PCC were not significantly impacted by irradiance or wind speed. Figure 10 displays the outcomes of the proposed hybrid RE system. The DVR and nonlinear load are switched on between 0.35 and 0.45 seconds.

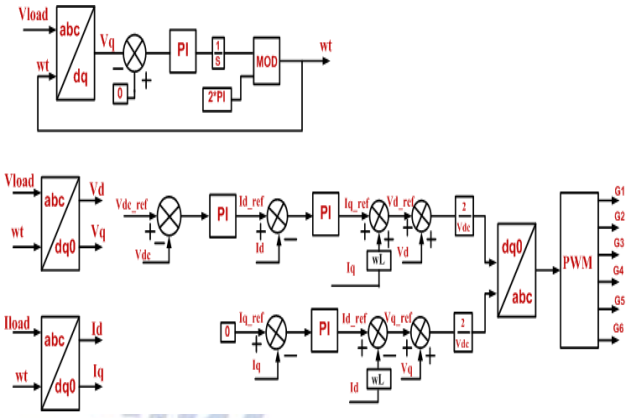

Fig. 5. Block diagram of inverter control

3. DVR Control

Initially, in this controlling method, in order to stabilize DC voltage and control of voltage of capacitor, the voltage of capacitor should be evaluated and compared with its basic value and the consequence of this comparison is deemed as the input for fuzzy controller 4. In fuzzy system, input of system is defined as equations given below:

$$e(t) = v^* - v_s$$

$$\Delta e(t) = e(t) - e(t-1)$$

v^* is reference signal and v_s is the signal to be regulated. With regard to the Park transform, the load voltage is divided to v_d and v_q perpendicular parameters. After Park Transform v_d and v_{dref} voltages are compared and the result of the comparison is considered as input of fuzzy controller 3. This controller is utilized to stabilize the real voltage. Parameters v_d and v_d are compared to v_{dref} And v_{qref} And the consequent is deemed as the input for fuzzy controller 1,2. Fuzzy controller 2 is used to stabilize the reactive voltage. Output of fuzzy controller 1,2,3 is given to generator pulses in order to produce switching signals, after Park inverse transform. In this controlling method PLL is used to synchronize the injection voltage with network voltage. Figure 6 depicts controlling block diagram of DVR system.

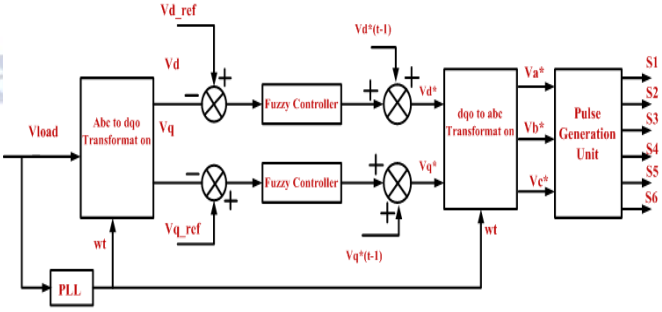

Figure .6. Depicts controlling block diagram of DVR system.

4. PROPOSED CONTROL SYSTEM

The fuzzy dials are easy to manipulate. Information gathering, processing, and output. At this stage, the information provided by input devices like switches, thumbwheels, etc. is transformed into membership functions and truth values. In the processing step, all of the rules are run, individual outcomes are generated, and then everything is merged. At the last stage, the combined output is transformed into a control output. While triangles are the most common shape used for membership functions, trapezoids and bell curves are also common. The quantity and distribution of curves is more crucial than the precise shape. Fuzzy control system design is simply an organised type of trial and error, and it is grounded in empirical methodologies. Typically, events unfold as follows: The inputs and outputs of the system, as well as the resources it requires to run, must be documented. It is important to record the fuzzy sets used as inputs. The guidelines need to be documented. Learn the steps to defuzzification. Make any necessary adjustments after running the test suite to ensure a fully functional system. Complete the paperwork so that manufacturing can begin.

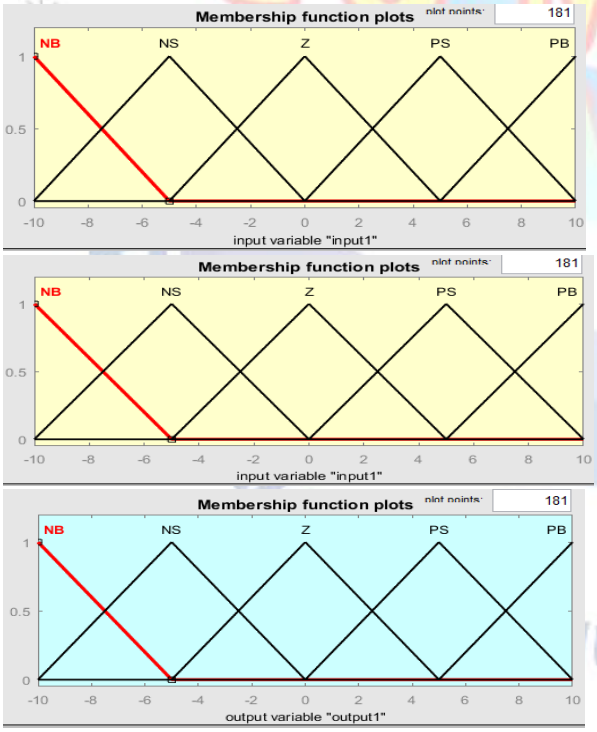

Fig 7 Example figures of input and output membership functions

There are three parts to this device. First, the Inputs are made fuzzy using input membership functions. Rule bases and an inference system are then used to get the final results. The system is then able to make advantage of the clarified fuzzy outputs. The variables selected are error and the rate of change in error. This is how the block model for fuzzy control looks:

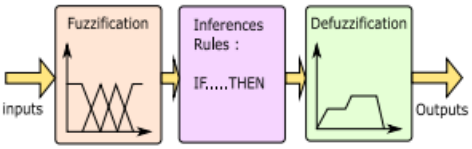

Fig. 8 shows the surface generated by the fuzzy system.

Table 1 Inference matrix

e / *de*	NB	NS	ZE	PS	PB
NB	NB	NB	NB	NS	ZE
NS	NB	NB	NS	ZE	PS
ZE	NB	NS	ZE	PS	PB
PS	NS	ZE	PS	PB	PB
PB	ZE	PS	PB	PB	PB

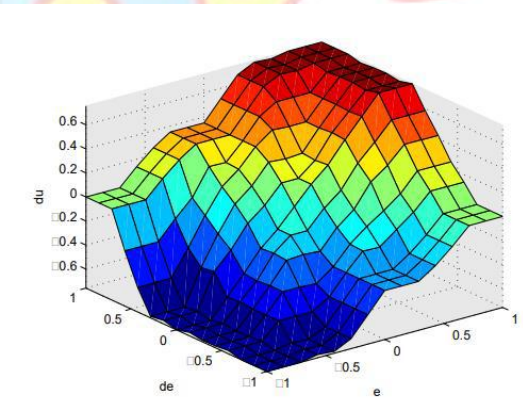

Fig. 9 Surface generated by the fuzzy system

While designing a fuzzy controller for electric motor control, it is necessary to choose parameters such as language variables, membership functions, inference method, and defuzzification approach. In a fuzzy controller, the inputs are the error and the derivative of the error, and the output is the actual instruction. Figure 7 depicts the application of triangular and trapezoidal membership functions to the inputs (error, error variation) and the output (input process), respectively.

The following fuzzy membership subgroups have been established: The scales employed in this context are the negative big (NB), negative small (NS), zero (ZE),

positive small (PS), and positive big (PB) scales. Fuzzy rules are grouped in Table 1 to show how they are used to map inputs to the controller's output.

5. SIMULATION RESULTS AND DISCUSSIONS

To evaluate the efficacy of the proposed solar PV based DVR system with fuzzy logic control for PV-wind hybrid battery energy sources (see Fig. 1). The Simpower system is used for the simulation. Symmetrical and asymmetrical voltage drops are generated by applying a fault at the PCC bus for 0.2 and 0.65 seconds in this simulated test.

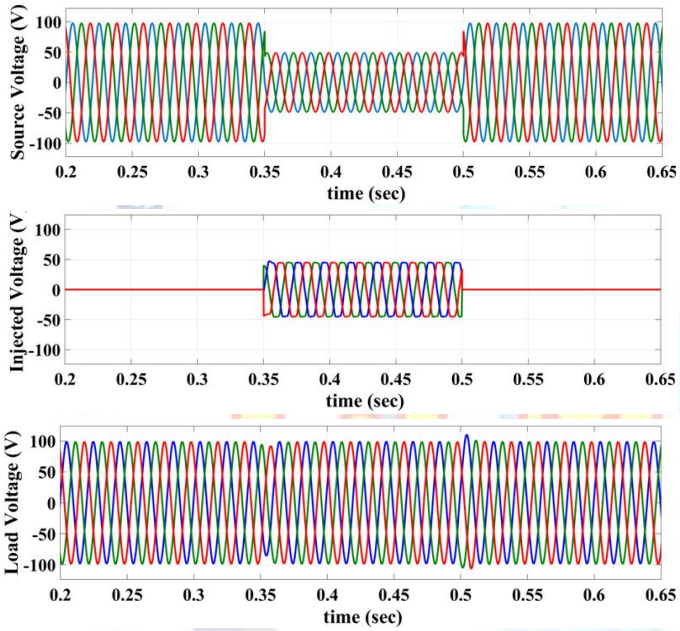

FIGURE 10. Simulation results and DVR response for 50% symmetrical voltage sag case (a) load voltage without DVR, (b) DVR injected voltage and (c) load voltage with DVR

As can be seen in Figure 10(a), the load voltage was cut in half. As can be observed in Fig. 10(c), the DVR system driven by solar panels greatly decreased the voltage drop. In addition, a change in phase appeared, ushering in a brand-new phase. The compensation simulation results show that, due to the switching scenarios at the beginning and end of the DVR's operational time, compensation is incomplete for a short while. Both symmetric and asymmetric voltage drops can occur in PV-wind power BESS systems, and they are not always caused by a malfunction. The intermittent nature of photovoltaic (PV) and wind power systems can lead to symmetrical sag, while a PV system connected to each phase can lead to asymmetrical voltage sag. The suggested solar PV based DVR will compensate for the power drop regardless of the source or the consistency with which it occurs. To demonstrate the effectiveness and robustness of the innovative control system, a stand-alone distributed generation system is developed and simulated in MATLAB/Simulink. In order to meet the load demands, the hybrid system runs at maximum efficiency. The combined output of solar photovoltaics (PV), wind turbines, and battery energy storage systems (BESS) is directly related to wind speed and sun radiation. Figure 11 illustrates this. This is when solar (PV) PMSG is operational on a consistent basis. Time intervals of t = 0.2s and t = 0.65s are required.

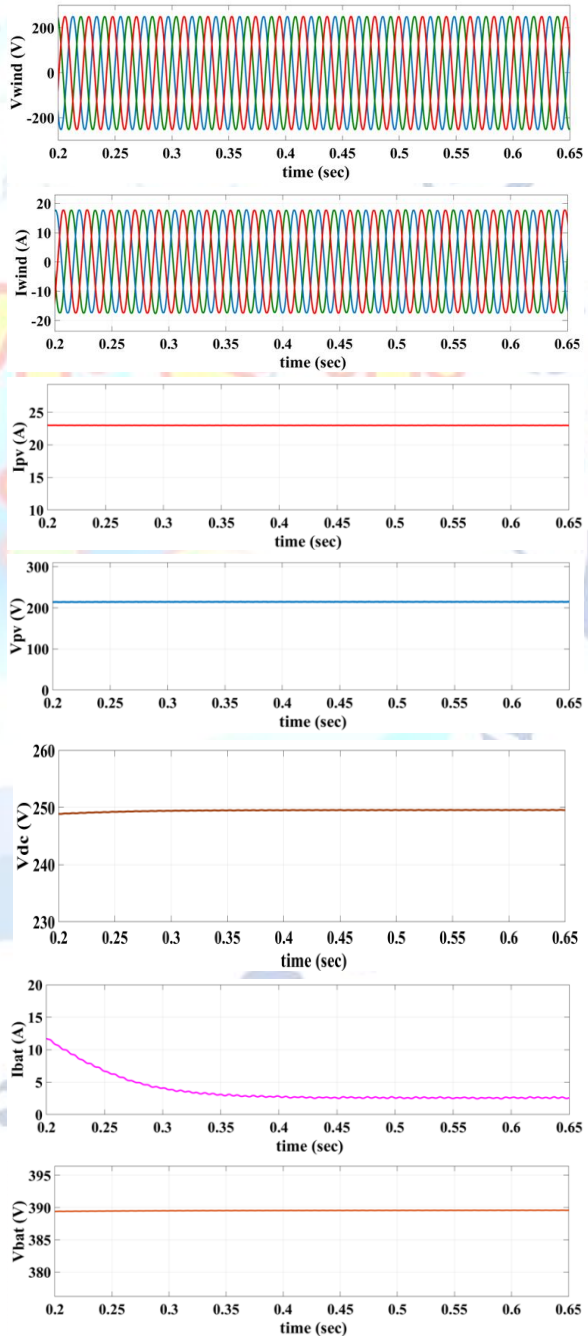

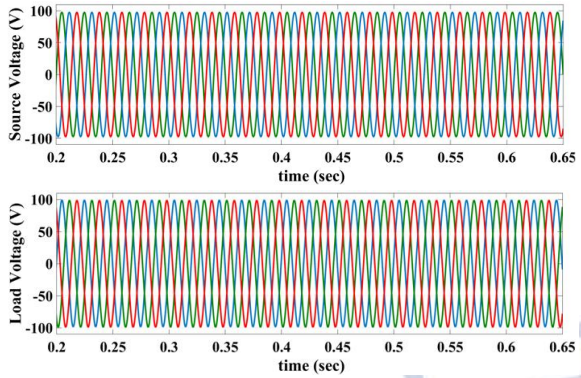

Fig. 11 wind voltage (Vwind), wind current (Iwind), solar current (Ipv), solar Voltage (Vpv), DC lin voltage (Vdc), battery current(Ibat) , battery voltage(Vbat), source voltage (V),load voltage (V).

6. CONCLUSION

This research shows how solar PV based DVR may be used to improve the voltage sag of a sensitive load that is supplied with power from a photovoltaic system, a wind energy system, and a battery storage system. The suggested DVR is intended to shield the sensitive load from voltage fluctuations caused by fault conditions or the unreliable output of PV-wind systems. In this research, we introduce a novel fuzzy control based DC-DC boost converter that, unlike some recently reported high DC voltage gain boost converters, uses a small number of components. DC voltage gain, voltage stresses, and conversion efficiency were all modelled for the proposed boost converter. The simulation findings validated the recommended layout. Furthermore, the proposed fuzzy based DVR system's full potential is unlocked through the development of the VSC's control and operation by monitoring the voltage level at the load. The ability to restore both magnitude and phase jumps is taken into account when deciding on a pre-sag compensation strategy. The proposed fuzzy based DVR operating states have been shown to be useful in real-world scenarios. The solar PV based DVR performs well in the simulation, which takes into account a variety of voltage sag depth situations for voltage imbalances. In subsequent works, we shall see examples of both voltage dips and voltage surges, as well as harmonics.

Conflict of interest statement

Authors declare that they do not have any conflict of interest.

REFERENCES

[1] BP Statistical Review of World Energy, 68th ed. 2019.

[2] M. R. Banaei and S. H. Hosseini, “Verification of a new energy control strategy for dynamic voltage restorer by simulation,” vol. 14, pp. 112–125, 2006.

[3] IRENA, Future of wind: Deployment, investment, technology, grid integration and socio-economic aspects (A Global Energy Transformation paper). International Renewable Energy Agency, Abu Dhabi, 2019.

[4] IRENA, Future of Solar Photovoltaic: Deployment, investment, technology, grid integration and socio-economic aspects (A Global Energy Transformation: paper). International Renewable Energy Agency, Abu Dhabi, 2019.

[5] H. M. Al-masri, S. Member, M. Ehsani, and L. Fellow, “Feasibility Investigation of a Hybrid On-Grid Wind Photovoltaic Retrofitting System,” IEEE Trans. Ind. Appl., vol. 52, no. 3, pp. 1979–1988, 2016.

[6] X. Xu, Z. Wei, Q. Ji, C. Wang, and G. Gao, “Global renewable energy development : In fl uencing factors , trend predictions and countermeasures,” Resour. Policy, vol. 63, no. April, 2019.

[7] E. Hache and A. Palle, “Renewable energy source integration into power networks , research trends and policy implications : A bibliometric and research actors survey analysis ☆,” Energy Policy, vol. 124, no. October 2018, pp. 23–35, 2019.

[8] M. Murshed, “Are Trade Liberalization policies aligned with Renewable Energy Transition in low and middle income countries ? An Instrumental Variable approach,” Renew. Energy, vol. 151, pp. 1110–1123, 2019.

[9] R. Mamat, M. S. M. Sani, F. Khoerunnisa, and A. Kadarohman, “Target and demand for renewable energy across 10 ASEAN countries by 2040,” Electr. J., vol. 32, no. 10, 2019.

[10] H. Qiao, F. Zheng, H. Jiang, and K. Dong, “Science of the Total Environment The greenhouse effect of the agriculture-economic growth-renewable energy nexus : Evidence from G20 countries,” Sci. Total Environ., vol. 671, pp. 722–731, 2019.

[11] IRENA (2019), RENEWABLE ENERGY MARKET ANALYSIS :GCC. IRENA, Abu Dhabi, 2019.

[12] G. Notton et al., “Intermittent and stochastic character of renewable energy sources : Consequences , cost of intermittence and bene fi t of forecasting,” Renew. Sustain. Energy Rev., vol. 87, pp. 96–105, 2018.

[13] A. Shivakumar, A. Dobbins, U. Fahl, and A. Singh, “Drivers of renewable energy deployment in the EU : An analysis of past trends and projections,” Energy Strateg. Rev., vol. 26, 2019.

[14] F. A. L. Jowder, “Design and analysis of dynamic voltage restorer for deep voltage sag and harmonic compensation,” IET Gener. Transm. Distrib., vol. 3, no. 6, pp. 547–560, 2009.

[15] S. Kim, S. Member, B. Kang, and S. Member, “Application of SMES and Grid Code Compliance to Wind / Photovoltaic Generation System,” IEEE Trans. Appl. Supercond., vol. 23, no. 2, 2013.

[16] S. Agalar and Y. A. Kaplan, “Power quality improvement using STS and DVR in wind energy system,” Renew. Energy, vol. 118, pp. 1031–1040, 2018.

[17] P. Kanjiya, B. Singh, A. Chandra, and K. Al-haddad, “‘ SRF Theory Revisited ’ to Control Self-Supported Dynamic Voltage Restorer (DVR) for Unbalanced and Nonlinear

Loads," IEEE Trans. Ind. Appl., vol. 49, no. 5, pp. 2330–2340, 2013.
[18] Z. Zheng, X. Xiao, X. Chen, C. Huang, L. Zhao, and C. Li, "Performance Evaluation of a MW-Class SMES-BES DVR System for Mitigation of Voltage," IEEE Trans. Ind. Appl., vol. 54, no. 4, pp. 3090–3099, 2018.
[19] A. M. Rauf and V. Khadkikar, "An Enhanced Voltage Sag Compensation Scheme for Dynamic Voltage Restorer," IEEE Trans. Ind. Electron., vol. 62, no. 5, pp. 2683–2692, 2015.
[20] G. Chen, M. Zhu, and X. Cai, "Medium-voltage level dynamic voltage restorer compensation strategy by positive and negative sequence extractions in multiple reference frames," IET Power Electron, no. December 2013, pp. 1747–1758, 2014.
[21] P. Jayaprakash, B. Singh, D. P. Kothari, A. Chandra, S. Member, and K. Al-haddad, "Control of Reduced-Rating Dynamic Voltage Restorer With a Battery Energy Storage System," IEEE Trans. Ind. Appl., vol. 50, no. 2, pp. 1295–1303, 2014.
[22] G. Dileep and S. N. Singh, "Selection of non-isolated DC-DC converters for solar photovoltaic system," Ren. and Sust. Energy Reviews, vol. 76, pp. 1230-1247, Oct. 2017.
[23] M. A. Ghasemi, A. Ramyar and H. Iman-Eini, "MPPT Method for PV Systems Under Partially Shaded Conditions by Approximating IV Curve," IEEE Tran. Ind. Electron., vol. 65, no. 5, pp. 3966-3975, May 2018.
[24] M. Kermadi, Z. Salam, J. Ahmed and E. M. Berkouk, "An Effective Hybrid Maximum Power Point Tracker of Photovoltaic Arrays for Complex Partial Shading Conditions," IEEE Tran. Ind. Electron., vol. 66, no. 9, pp. 6990-7000, Sept. 2019.
[25] H. Li, D. Yang, W. Su, J. L and X. Yu, "An Overall Distribution Particle Swarm Optimization MPPT Algorithm for Photovoltaic System Under Partial Shading," IEEE Tran. Ind. Electron., vol. 66, no. 1, pp. 265-275 Jan. 2019.
[26] K. S. Tey and S. Mekhilef, "Modified Incremental Conductance Algorithm for Photovoltaic System Under Partial Shading Conditions and Load Variation," IEEE Tran. Ind. Electron., vol. 61, no. 10, pp. 5384-5392, Oct. 2014.
[27] R. Ahmad, A. F. Murtaza and H. A. Sher, "Power tracking techniques for efficient operation of photovoltaic array in solar applications-A review," Renewable and Sustainable Energy Reviews, vol. 101, pp. 82-102, 2019.
[28] Pires, V.F.; Cordeiro, A.; Foito, D.; Silva, J.F. High Step-Up DC-DC Converter for Fuel Cell Vehicles Based on Merged Quadratic Boost-Cuk. IEEE Trans. Veh. Technol. 2019, 68, 7521–7530. [CrossRef]
[29] Zhang, Y.; Liu, H.; Li, J.; Sumner, M.; Xia, C. DC–DC Boost ConverterWith aWide Input Range and High Voltage Gain for Fuel Cell Vehicles. IEEE Trans. Power Electron. 2018, 34, 4100–4111. [CrossRef]
[30] Ferdowsi, A.A.M.; Shamsi, P. High-Voltage-Gain DC-DC Step-Up Converter with Bifold Dickson Voltage Multiplier Cells. IEEE Trans. Power Electron. 2019, 34, 9732–9742.
[31] F. Blaabjerg, Z. Chen and S. B. Kjaer, " Power Electronics as Efficient Interface in Dispersed Power Generation Systems ", IEEE Transactions on Power Electronics, vol. 19, no. 5, pp.1184-1194, 2004.
[32] A. Mohamed, M. Elshaer and O. Mohammed, " Bi-Directional AC-DC/DC-AC Converter for Power Sharing of Hybrid AC/DC Systems ", IEEE Power and Energy Society General Meeting, pp. 1-8, 2011.